K-shell internal conversion coefficient for *M*4 decay of the 30.8 keV isomer in ^{93}Nb

V. Horvat,* E. E. Tereshatov, J. C. Hardy,† N. Nica, C. M. Folden III, and V. E. Iacob
Cyclotron Institute, Texas A&M University, College Station, Texas 77843, USA‡

M. B. Trzhaskovskaya
Petersburg Nuclear Physics Institute, Gatchina 188300, Russia

(Received 14 May 2020; accepted 30 June 2020; published 13 July 2020)

The 30.8 keV $(1/2)^-$ isomeric state in $^{93}_{41}$Nb decays by an *M*4 transition to the $(9/2)^+$ ground state. We have measured the *K*-shell internal conversion coefficient α_K for this transition in order to test the validity of current methods of calculation for a case with relatively low atomic number, low transition energy, and a high value of α_K. Taking the fluorescence yield of niobium to be 0.751(4), we obtain $\alpha_K = 2.56(9) \times 10^4$, a result that agrees with the Dirac-Fock calculations that take into account the presence of a *K* vacancy in the final state, and disagrees by 1.7 standard deviations with calculations that ignore the vacancy. We also determine the energy of the isomeric state to be 30.760(5) keV, a fourfold improvement in precision over the currently accepted value.

DOI: 10.1103/PhysRevC.102.014310

I. INTRODUCTION

Internal conversion coefficients (ICCs) are essential in the analysis of nuclear decay schemes. Their values are used to determine the spins and parities of energy levels, as well as branching ratios, transition rates, and transition multipolarity mixing ratios. The accuracy of nuclear level schemes is especially important for nuclides used in detector efficiency calibrations.

Nevertheless, the systematic quest for highly accurate values of the ICCs started only in 2002, following development of a computer code built within the Dirac-Fock framework, which for the first time accounted exactly for exchange interactions among the bound electrons, and between those electrons and the electron ejected during the conversion process [1]. This improved the accuracy of the calculations for high-multipolarity transitions and drew attention to the problem of how to deal with the atomic vacancy left behind by the ejected atomic electron.

Prior to 2002, some ICC calculations took account of the vacancy, while others did not (see Ref. [2] for a detailed comparison of the underlying assumptions for various ICC tabulations). In producing their published tables, Band *et al.* [1] chose to use a calculation that ignored the vacancy, stating that there was no compelling experimental evidence to warrant its inclusion. This choice was borne out by an exhaustive comparison of ICC calculations with world experimental data, which appeared concurrently [2] and showed a slight preference for the no-vacancy calculation. However, world data available at the time included very few measurements of sufficient precision to discriminate meaningfully between the vacancy and no-vacancy calculations. More significantly, atomic vacancy lifetimes were known [3] to be considerably longer than the time the conversion electron takes to leave the vicinity of the atom, which contradicts the assertion that the vacancy can be ignored in the conversion process.

To settle the issue, new precise ICC measurements were needed. Inclusion of the atomic vacancy generally increases the calculated ICC values [2] and, although the effects are usually rather small, they can be quite significant in cases with high multipolarity and a low kinetic energy of the ejected electron [4]. With careful selection of the transitions to be studied, ICC measurements can discriminate between the vacancy and no-vacancy calculations.

To date, we have performed nine highly precise measurements of the *K*-shell internal conversion coefficient, α_K, involving *E*3 or *M*4 transitions in ^{193}Ir [5,6], ^{134}Cs and ^{137}Ba [7,8], ^{197}Pt [9], ^{119}Sn [4], ^{111}Cd [10], ^{125}Te [11], ^{127}Te [12], and ^{103}Rh [13]. The results from these measurements were reviewed most recently in Ref. [14], along with the only three equivalently precise measurements performed elsewhere, on transitions in ^{113}In [2], ^{115}In [15], and ^{197}Hg [16]. They all agree better with calculations that account for the atomic vacancy in the final state. The new measurement presented here, of the *M*4 isomeric transition in ^{93}Nb, represents the lowest atomic number, the lowest transition energy,[1] and the highest α_K value that we have measured so far.

There have been two previous measurements of α_K for the 30.8 keV *M*4 transition in ^{93m}Nb, both published more than 40 years ago. One [17] obtained $\alpha_K = 2.58(15) \times 10^4$ and the other [18] $\alpha_K = 1.7(3) \times 10^4$. Not only are they in serious

*V-Horvat@tamu.edu
†Hardy@tamu.edu
‡http://cyclotron.tamu.edu/

[1]Though not the lowest-energy conversion electrons. That record remains with the *M*4 transition in ^{193}Ir.

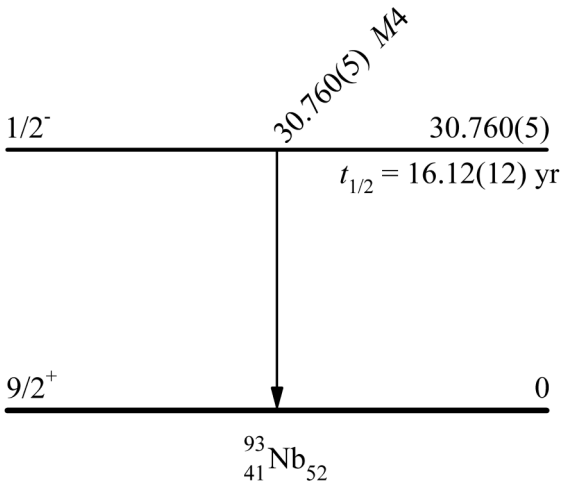

FIG. 1. The decay scheme of ^{93m}Nb [19], in which we have incorporated our new value for the transition energy, given in keV.

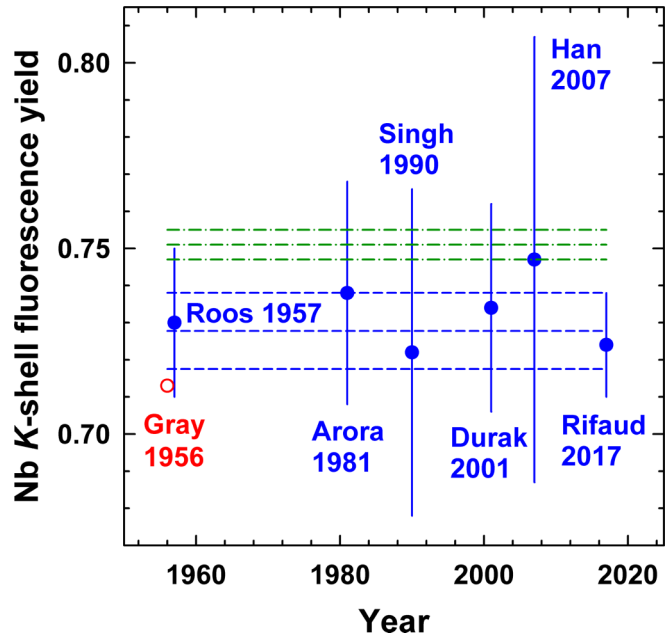

FIG. 2. World data for the niobium K-shell fluorescence yield; the references in chronological order are [20–26]. Those results with quoted uncertainties appear as solid blue circles with error bars. Their weighted average and the corresponding uncertainty limits appear as dashed blue lines. The result without uncertainty (red open circle) is not included. Shown with the green dot-dashed lines is the result for niobium based on a systematic evaluation of all elements with $10 \leqslant Z \leqslant 100$ [27], along with its uncertainty limits.

disagreement with one another, but neither is precise enough to distinguish clearly between the vacancy and no-vacancy calculations, even though the two calculated results differ by more than 6.2%.

We have measured α_K for the ^{93}Nb transition with an uncertainty of 3.7% (limited predominantly by counting statistics), which is nearly a factor of two more precise than the best of the previous measurements. This turns out to be quite sufficient to distinguish between the two types of calculations. We also report a new and improved result for the $M4$ transition energy.

II. METHOD

The 30.8 keV $(1/2)^-$ isomer in ^{93}Nb is the first excited state of that nuclide and has a half-life of about 16 yr. It decays to the $(9/2)^+$ ground state by an $M4$ transition. K-shell internal conversion of the transition is energetically allowed, leaving about 12 keV for the final kinetic energy of the converted electron. A K x ray of niobium is emitted as the atomic K vacancy gets filled by an electron from a higher shell. The decay scheme of ^{93m}Nb is shown in Fig. 1.

Under these conditions, if a spectrum of K x rays and γ rays is measured with the same detector, the K-shell internal conversion coefficient α_K for the transition is given by

$$\alpha_K = \frac{N_K}{N_\gamma}\frac{\epsilon_\gamma}{\epsilon_K}\frac{1}{\omega_K}, \tag{1}$$

where ω_K is the niobium K-shell fluorescence yield; N_K and N_γ are the total numbers of observed K x rays and γ rays, respectively; and $\epsilon_\gamma/\epsilon_K$ is the detector efficiency for the γ rays relative to its efficiency for the K x rays.

The niobium K-shell fluorescence yield has been measured seven times in the past [20–26]. The results are listed in Ref. [26] and shown in Fig. 2. Their weighted average is 0.728(10), with a relative uncertainty of ±1.4% and a small reduced χ^2 of 0.073. However there is a competing value for the fluorescence yield for niobium. It comes from an evaluation by Schönfeld and Janssen [27] of all world data for ω_K in elements with $10 \leqslant Z \leqslant 100$. The authors made a systematic analysis of the results, from which they recommended ω_K values for all the elements within the range. Based on this broader data set, with significant influence from the data for neighboring elements, the value they recommended for niobium, $Z = 41$, is 0.751(4). This value with its assigned uncertainty appears as dot-dashed lines in Fig. 2.

Note in the figure that the most recent measurement [26] has the smallest uncertainty and dominates in the calculation of the experimental average; moreover, it is the only result to be statistically inconsistent with the systematic-analysis value. Nevertheless, there is no objective reason to discount it.

Both values for the fluorescence yield have their merits but, as they do not agree with one another, we are forced to make a choice between them in presenting our result for α_K. We have elected to use the value from the systematic analysis of Schönfeld and Janssen principally to maintain consistency with our previous work, in which we have always used their recommended values. Furthermore, as will become clear in Sec. V, this is the most conservative choice we could make in the context of our selecting between the two theoretical predictions for α_K. The conclusion we reach using our preferred systematic value for ω_K is even more convincingly reached if the average experimental ω_K value is used.

The remaining quantities on the right-hand side of Eq. (1) have been measured directly. The details will be given in Secs. III and IV.

III. EXPERIMENT

A. Source preparation and quality assessment

We purchased a solution of ^{93m}Nb in 1 M HNO_3 + 0.3 M HF from Eckert and Ziegler Products and used it to prepare thin ^{93m}Nb sources by means of the molecular electroplating technique [28]. Specific details of the chemical and electrochemical procedures followed in this work will appear in a separate publication, so we will only give a summary here.

Before working with active material, we developed and optimized our procedures using a nonradioactive niobium solution (1 mg/mL in nitric acid). The efficiency of niobium electrodeposition was optimized at a current density of 3–5 mA/cm^2 by careful purification of the main organic solvent in the target cell (isopropanol) and the source backing (a 2-cm-diameter, 12-μm-thick aluminum foil), specifically by electrochemical removal of water from the solvent and the oxide layer from the backing. The prepared samples were characterized at the Materials Characterization Facility of Texas A&M University by means of scanning electron microscopy (SEM), energy dispersive spectroscopy (EDS), and x-ray photoelectron spectroscopy (XPS), as well as by visual inspection of the color of the deposited layer. SEM was used to verify the samples' uniformity by demonstrating that there were no significant cracks or craters, nor any flaking or peeling; the remaining three procedures confirmed that niobium was deposited in the form of pentoxide, Nb_2O_5.

The electrodeposition method we employed is known to be limited to a maximum of 1–2 mg/cm^2 of deposited material in order to maintain the integrity of the film. Therefore, to increase the activity of the source, we chose to make its radius as large as possible with the given target cell. At peak efficiency the procedure was completed in about 15 h.

A total of five sources were made, each having a different thickness and hence different activity. The strongest source—the one we ultimately used in our measurement—had a mass of 3.0 mg, as determined from the difference between the mass of the bare backing material and its mass after the niobium pentoxide had been deposited. The source diameter (17 mm) was measured directly. This information was used to deduce the mass thickness of the source (1.3 mg/cm^2).

To identify any radioactive contaminants that might be present, we placed each source 15.1 cm in front of our HPGe detector, the distance at which the detector has been precisely calibrated [30]. The room background was also measured under the same conditions, but in the absence of the source. Shown in Fig. 3 is a background-subtracted spectrum from our strongest source.

The only radioactive impurity that we observed, ^{94}Nb, has a half-life of about 2×10^4 yr and β decays exclusively to the 1574 keV level of ^{94}Mo. That level de-excites to the ground state via two $E2$ γ rays in cascade (at 702.6 keV and 871.1 keV), which are clearly seen in the spectrum along with the peak at 1574 keV due to their coincidence summing. K-shell internal conversion of the two γ rays is negligible

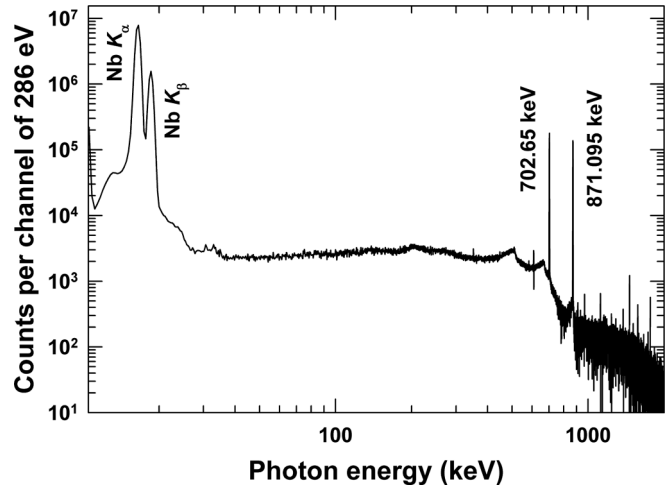

FIG. 3. The net spectrum of x rays and γ rays from our ^{93m}Nb source, taken with our HPGe detector [30]. The spectrum is dominated by the K_α and K_β x rays of niobium. The two labeled peaks are due to γ rays from the decay of the ^{94}Nb contaminant. The narrow upward and/or downward spikes are artifacts of the background subtraction, occurring at the location of peaks in the background spectrum. Note the cluster of small unresolved peaks near 30 keV.

($\alpha_K = 1.608 \times 10^{-3}$ and 9.39×10^{-4}, respectively), and so is the contribution to the spectrum from the corresponding molybdenum K x rays. We estimate that for our samples the detection rate of Mo K x rays divided by the detection rate of Nb K x rays is less than 2×10^{-4}.

The activity of ^{93m}Nb in the source was found to be about 1.28×10^5 Bq (3.57 μCi), while that of ^{94}Nb was determined to be about 1% of that amount. Considering that the emission rate of ^{94}Nb γ rays is low and that our source is relatively thin, we expect that the contribution from fluorescence to the niobium K-x-ray peaks in the spectrum is negligible as well.

While only the strongest of the five sources was used in the ICC measurements, all five were used to establish that the sources did not contain significant quantities of stable substances. We did this by measuring the intensity of the niobium K x rays relative to that of the high-energy ^{94}Nb γ rays. Since the five sources all had different thicknesses, we would expect the intensity ratio to decrease with increasing thickness if substantial amounts of inactive material had accumulated along with the two active niobium isotopes. Instead, the ratios were found to be identical within statistics, thus confirming the absence of significant inactive impurities.

Having eliminated the possible influence of inactive material in the source, we calculated the effects of absorption within the active source material (self-absorption) based on the standard tables of absorption coefficients [29]. For a layer of niobium pentoxide 1.3 mg/cm^2 thick, we found that absorption of the 30.8 keV γ rays was greater than that of the niobium K x rays by a factor of 1.0026(13). The uncertainty incorporates a provision for possible microscopic nonuniformity in the source thickness, which we conservatively estimated to be ±20%. Though small compared to our ultimate statistical uncertainty, for completeness we incorporated this correction in our analysis.

B. Measurement of x-ray and γ-ray spectra

In all our previous measurements [4–14] we have used our well-calibrated HPGe detector [30], but that proved to be inadequate in this case for two main reasons: (*i*) the efficiency of the HPGe detector for niobium K x rays (at 16.5 keV–19.0 keV) is much lower than its efficiency for the 30.8 keV γ rays and is not well characterized, which leads to a large uncertainty in the relative efficiency $\epsilon_\gamma/\epsilon_K$ needed for Eq. (1); and, more importantly, (*ii*) random summing of niobium K_α x rays results in peaks of similar magnitude that are unresolved from the 30.8 keV γ-ray peak (see Fig. 3), making it impossible to determine N_γ with sufficient accuracy. So instead, we used a lithium-drifted silicon detector [Si(Li)], which is designed for use in this energy region, has superior energy resolution (310 eV FWHM at 31 keV), and has an efficiency that is less dependent on energy in the range of 16–31 keV [31].

Signals from the Si(Li) detector's preamplifier were amplified and then passed to an EASY-MCA^{TM} 8k multichannel analyzer [32] controlled by MAESTRO^{TM} software [33]. The acquired spectra were stored on the personal computer that hosted the software.

The data acquisition rate was limited to about 50 events per second mainly by the emission rate from the source at hand but also by our selection of the most appropriate source-to-detector distance (12.1 mm) based on the size of the source and the structure of our Si(Li) detector, which will be discussed in Sec. IV C. Under these conditions the detection rate of the 30.8-keV ^{93m}Nb γ rays was about 4 per hour. Consequently, to reduce the statistical uncertainty, the spectrum was accumulated over a time period of several months. However, the spectrum was saved at least once per day and whenever the measurement was interrupted, for example to make a background or calibration measurement.

Figure 4 shows the spectrum of photons emitted from our ^{93m}Nb source, acquired over a period of 156 d, from which we determined N_K and N_γ as needed for Eq. (1). We refer to this as spectrum A. An additional measurement was performed for another 29 d at the closest possible source-to-detector distance (resulting in spectrum B, a portion of which appears in Fig. 5) in order to enhance the statistics for the γ-ray peak so we could determine its energy centroid with better precision. This is important because the calculated value of α_K depends strongly on the transition energy, and its uncertainty is derived from the uncertainty in that energy.

C. Energy calibration of the measured spectra

Considerable effort was made to ensure stability and reliability of the energy scale associated with the measured photon spectra. This was accomplished by our performing strategically interspersed measurements with calibration sources of ^{241}Am and ^{109}Cd, from which we determined the centroids of selected peaks that ranged in energy from 11 870.8(21) eV (the neptunium L_l x ray from ^{241}Am [34]) to 88 033.6(10) eV (the ^{109m}Ag γ ray following the ^{109}Cd β decay [35]). Using this information we determined the energy scale individually for every spectrum obtained in an uninterrupted measurement and then put all these spectra on a common energy scale by means of rebinning. No evidence of nonlinearity was found, so all scale transformations were strictly linear. Because all the individual energy scales were close to 10 eV per channel, the common scale was set to exactly 10 eV per channel. For the final analysis, the individual rebinned spectra obtained under equivalent experimental conditions were combined into a single spectrum.

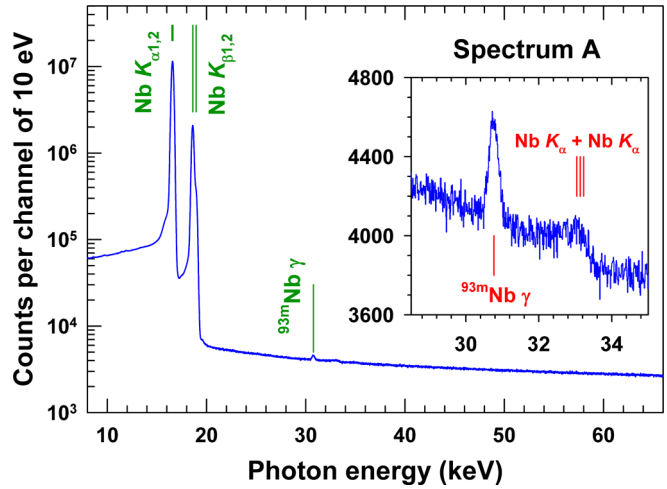

FIG. 4. Spectrum of photons emitted from the ^{93m}Nb source (spectrum A) taken with our Si(Li) detector, from which we determined N_K and N_γ [see Eq. (1)]. The insert provides a more detailed view of the 30.8 keV γ-ray peak as well as the broad peak due to random summing of niobium K_α x rays. The two peaks are obviously well resolved from each other. There is no significant contribution to the spectrum from the K conversion electrons (at 11.8 keV) and no indication of peaks due to L conversion electrons (at about 28 keV). Therefore, no peaks due to detection of $M+$ conversion electrons are expected either, and none were found.

IV. ANALYSIS

A. Transition energy

To establish a precise and accurate energy for the 30.8-keV isomeric transition in ^{93m}Nb we used four calibration points, which are all presented in Table I. The first two involve K_α x rays of niobium (from the ^{93m}Nb source) and K_α x rays of silver (from the ^{109}Cd source). Since in both cases the $K_{\alpha 1}$ and $K_{\alpha 2}$ peaks are unresolved from one another, we use the intensity-weighted average energies (see Table I), which are known with uncertainties of only ± 0.27 and ± 0.20 eV, respectively. These two composite peaks are well resolved from any other peaks, contain on the order of 10^8 events, and lie on a relatively low background, so that their centroids could be determined with uncertainties of only ± 0.15 eV and ± 0.07 eV, respectively.

The remaining two energy-calibration points were provided by the $K_{\alpha 1}$ x ray of lanthanum and the ^{237}Np γ ray at 26.34 keV (both from the ^{241}Am source). Lanthanum was present in the ^{241}Am source or its backing as an impurity in sufficient quantity to produce prominent K x-ray peaks in the spectrum by means of fluorescence. Peaks due to $K_{\alpha 1}$ and $K_{\alpha 2}$ x rays of lanthanum were well resolved from each

TABLE I. Calibration data and fit results used to determine the energy of the ^{93m}Nb γ ray. Symbols E, I, and C denote energy, intensity, and centroid, respectively. The centroids are given in channel units.

Quantity	Value	Source
Niobium K_α x rays		
E(Nb $K_{\alpha1}$)	16 615.16(33) eV	[34]
E(Nb $K_{\alpha2}$)	16 521.28(33) eV	[34]
$\frac{I(\text{Nb } K_{\alpha2})}{I(\text{Nb } K_{\alpha1})}$	0.5236(26)	[36]
E(Nb K_α)	16 582.90(27) eV	weighted average
Silver K_α x rays		
E(Ag $K_{\alpha1}$)	22 162.917(30) eV	[34]
E(Ag $K_{\alpha2}$)	21 990.30(10) eV	[34]
$\frac{I(\text{Ag } K_{\alpha2})}{I(\text{Ag } K_{\alpha1})}$	0.5305(27)	[36]
E(Ag K_α)	22 103.08(20) eV	weighted average
Other calibration lines		
E(^{237}Np γ)	26 344.6(2) eV	[19]
E(La $K_{\alpha1}$)	33 442.12(27) eV	[34]
Centroid measurements		
C(Nb K_α)	1657.236(15)	fit
C(Ag K_α)	2209.771(7)	fit
C(^{237}Np γ)	2634.17(1)	fit
C(La $K_{\alpha1}$)	3344.33(3)	fit
C(^{93m}Nb γ)	3075.94(42)	fit
Derived energy of ^{93m}Nb γ ray		
E(^{93m}Nb γ)	30 760(5) eV	

other. However, a relatively small peak (accounting for less than 9% of the events), from the ^{237}Np γ ray at 33.20 keV, was not resolved from the lanthanum K_α doublet. We took it properly into account by referring to a spectrum separately measured using a secondary ^{241}Am source that did not contain any impurity peaks around 33.20 keV.

The centroid of the ^{93m}Nb γ-ray peak was obtained from spectrum B. The quality of the fit is illustrated in Fig. 5. The peak was fitted with a single Gaussian on a linear background, as shown. The centroid result, which appears in Table I, was found to be stable against changes in the fitting region. We determined the corresponding energy by using the scale based on the four calibration points described above. All relevant results from this analysis are given in Table I. The result we finally obtain for the ^{93m}Nb γ-ray energy is

$$E_\gamma = 30\,760(5)\ \text{eV}. \tag{2}$$

The quoted uncertainty includes the statistical uncertainty of the peak centroid, as well as a minor contribution from uncertainty in the energy scale. Our result is in agreement with the currently accepted value of 30.77(2) keV [19], but its uncertainty is smaller by a factor of four.

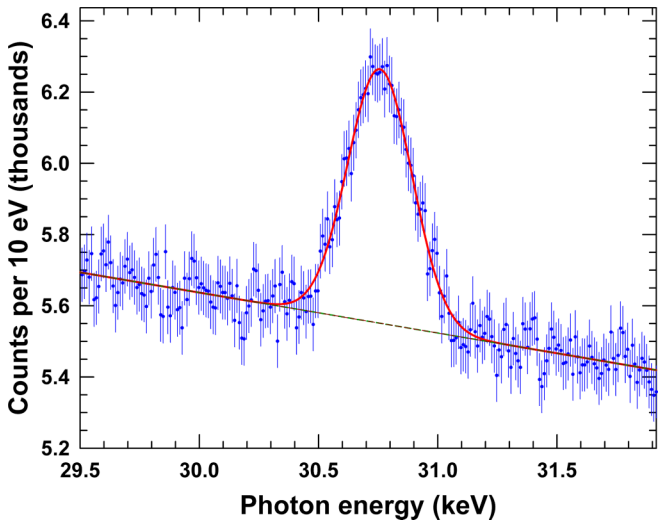

FIG. 5. Fit to the ^{93m}Nb γ-ray peak of spectrum B.

B. Determination of N_γ and N_K from the measured spectra

The peaks of interest in the measured spectra were analyzed with software that we wrote and specifically customized for the present application. The software employs a fitting function that includes skewed Gaussian peaks, i.e., Gaussians with exponential tails restricted to their low-energy side. Each peak is also associated with a specific linear "peak background" that is restricted to the low-energy side of the peak centroid and is convoluted with an appropriate normalized Gaussian function. This background is primarily due to x-ray scattering. The overall "spectral background" (deemed to be present in the absence of the peaks) is modeled as a linear function of energy. To calculate the number of events in a given channel, the fitting function is integrated between that channel's limits.

As is evident from Fig. 5, it was straightforward to fit the ^{93m}Nb γ-ray peak with a single Gaussian component, yielding $N_\gamma = 1.584(56) \times 10^4$ for spectrum A. Dealing with the K x-ray peaks proved to be much more challenging. Fortunately, for them the peak-to-background ratio is relatively high, so the result is rather insensitive to the details of the fit. We used the model illustrated by Fig. 6, in which the four principal components (shown in blue) represent full-energy peaks corresponding to the niobium $K_{\alpha2}$, $K_{\alpha1}$, $K_{\beta1,3}$, and $K_{\beta2'}$ x rays, while the remaining four wider peaks (shown in purple) act as their "shadows", having intensities smaller by the same proportion, and energies reduced by the same small amount. The primary role of the shadow peaks is to account for incomplete charge collection in the detector and radiative Auger (RA) transitions, but they also improve accuracy of the fit of a spectrum that features Voigt-shaped peaks.[2] All eight peak components are consistently described by skewed Gaussians. In Fig. 6 the background in the absence of the

[2]The shape of a measured full-energy x-ray peak is best described by a Voigt function, the convolution of a Lorentzian-function line profile and a Gaussian-function detector response [39]. In our measurements, the line widths are less than 4% of the detector peak widths, so the deviation from Gaussian shape is very small. Contributions from radiative Auger transitions are on the order of 1% for the K x rays of niobium and silver [37,38].

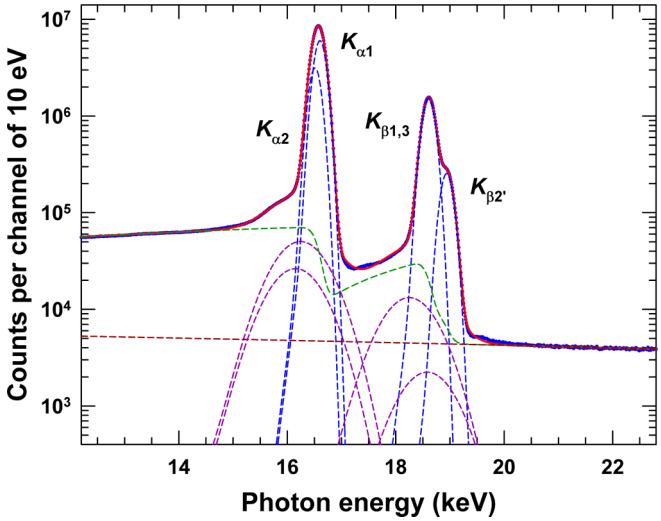

FIG. 6. Illustration of the model used to describe the niobium K x-ray peaks. See text for the details. The data are from the last uninterrupted measurement with the ^{93m}Nb source. The same model was also used to analyze the silver K x rays emitted by our ^{109}Cd calibration source.

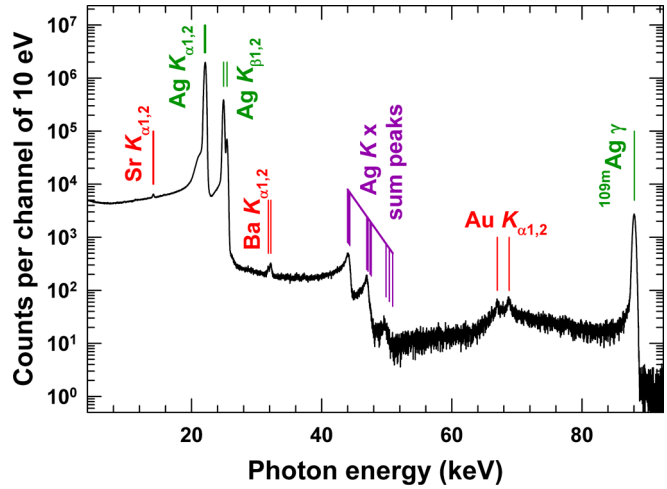

FIG. 7. Spectrum of photons emitted from the ^{109}Cd source, taken with our Si(Li) detector. Besides the peaks due to the 88.03 keV γ ray and the four characteristic K x rays of silver ($K_{\alpha 1}$, $K_{\alpha 2}$, $K_{\beta 1,3}$, and $K_{\beta 2'}$), also prominent are the random summing peaks from coincident detection of two characteristic K x rays of silver. The remaining labeled peaks are due to $K_{\alpha 1,2}$ x rays of strontium, barium, and gold. These peaks are not present in the spectrum taken with the ^{93m}Nb source and so they must originate from the ^{109}Cd source itself.

peaks is shown in brown, while the combined background is shown in green.

To extract the energy of a peak for the purpose of energy calibration we used the centroid of the Gaussian component of the principal peak, disregarding its exponential tail. However, to obtain the number of counts associated with a peak we included its full profile: i.e., the counts in the Gaussian component of the peak, its exponential tail and its "shadow" peak. This convention, which we believe is the most appropriate one, was used for the K x rays of both niobium and silver. The measured number of the former is needed to determine N_K of Eq. (1) and that of the latter is needed to determine the efficiency of the detector (see Sec. IV C). Had we used a different convention and applied it consistently to both sets of peaks, N_K and ϵ_K of Eq. (1) would have been different by a similar fraction, leaving their ratio essentially unchanged. The result we obtain from spectrum A is $N_K = 4.1935(23) \times 10^8$.

C. Efficiency calibration of our Si(Li) detector

The energy-dependent efficiency of our Si(Li) detector was determined from measurements involving two calibration sources: a ^{109}Cd source purchased from Eckert & Ziegler Products, having a specified reference activity of 170.8(17) kBq as of July 15, 2018; and a legacy ^{241}Am source with a measured activity of about 105 kBq. While the latter was used as our primary ^{241}Am source, we also made use of a secondary ^{241}Am source for specialized purposes (see Secs. IV A, IV C 2, and IV C 3).

In overview, our procedure was to focus on detection efficiencies of several key x rays and γ rays that contribute to the measured spectra, and then reproduce them with the CYLTRAN Monte Carlo electron-and-photon transport code [40] calculations. The geometric data we input to the code specified the space occupied by all relevant materials comprising and surrounding the source and the detector. All dimensions we could measure were fixed, but unmeasurable internal dimensions, such as the distance between the silicon crystal and the beryllium window of the detector assembly, were adjusted to optimize agreement with the calibration-source data. The final set of common geometric input data was then applied to the counting setup used for the ^{93m}Nb source in order to calculate $\epsilon_\gamma/\epsilon_K$, the efficiency ratio required for Eq. (1). The details of these calibration procedures are provided in the following sections.

1. *Efficiency measurements and data analysis*

Figure 7 shows the spectrum we acquired with the ^{109}Cd source placed at a caliper-measured source-to-detector distance of 10.2 mm. The absolute efficiencies of the detector were obtained for the K x rays of silver, which have an average photon energy of 22.61 keV, and for the 88.03 keV γ rays, based on the measured numbers of counts in the corresponding peaks, the known live time of the acquisition, and the derived activity of the source at the time of the measurement. The reference data we used for the number of K x rays and γ rays per ^{109}Cd decay were the same as those used in Ref. [4]. We designate these measured efficiencies for the 22.61-keV x rays and the 88.03-keV γ rays as ϵ_{23} and ϵ_{88}, respectively.

Another measurement was also made with the same source at the source-to-detector distance of 0.8 mm (the shortest distance allowed by the source mount), from which we determined the corresponding absolute efficiencies ϵ'_{23} and ϵ'_{88}. The reason for measuring the ^{109}Cd at two distances will become clear in Sec. IV C 3.

From our measured photon spectrum of the ^{241}Am source, which was obtained at the source-to-detector distance of 15.9 mm (also the shortest distance allowed by its mount), we determined the ratio of efficiencies $\epsilon_{12}/\epsilon_{60}$ for the 11.89-keV neptunium L_l x rays and the ^{237}Np 59.54-keV γ rays. Compared to our ^{109}Cd source, the ^{241}Am source had a considerable thickness and a significantly higher atomic number. Therefore, because of the low energy of the x rays, we had to correct our measured efficiency ratio for absorption within the source. The correction factor was determined in a separate series of measurements, the details of which are given in Sec. IV C 2.

Note that no silicon K x-ray escape peaks (shifted down by about 1.74 keV relative to the full-energy peaks) were observed in any of the spectra that we measured. This is best illustrated by Fig. 6, but is also confirmed by Figs. 4 and 7. Consequently, any effects from escape were considered to be negligible.

2. *Measurements of self-absorption in* ^{241}Am

To measure the self-absorption of photons emitted from our primary ^{241}Am source we used a special source holder that let us accurately position the source at a known angle relative to the plane of the detector window. We placed the source at a distance of 15.9 mm from the detector and recorded spectra at various angles θ between -60° and $+60^\circ$ in steps of 15°, from which we extracted the areas of the 11.89- and 59.54-keV peaks. We then examined the dependence of their area ratio on the source angle. That ratio should decrease with angle according to $\exp[-x\Delta\mu/\cos(\theta)]$, where $\Delta\mu$ is the difference between the known [41] absorption coefficients in americium at photon energies of 11.89 keV and 59.54 keV, and x is the source thickness. By least-squares fitting the data we determined x to be 263 μg/cm^2, which corresponds to a self-absorption correction factor of 1.032(2).

We determined the thickness of our secondary ^{241}Am source simply by comparing its 11.89-to-59.54 keV peak ratio to that of our primary source at zero degrees. Its thickness was thus determined to be 563 μg/cm^2; and its correction factor for $\epsilon_{12}/\epsilon_{60}$ becomes 1.069(5).

To calculate the relative self-absorption correction factors for the remaining peaks in the spectra from both sources, we used their respective source thicknesses and the known values of absorption coefficients [41] at the relevant energies.

3. *Efficiency calculations*

Initially, geometric modeling of the detector was based on our external measurements, the manufacturer's specifications, and some additional (mostly qualitative) information obtained from the manufacturer. However, these led to calculated efficiencies that were much larger than those determined experimentally. This is not surprising and can be attributed principally to aging of the detector [42], which leads to a gradual reduction in the active volume of the cylindrical silicon crystal. We modeled this effect by introducing d_F, the thickness of the silicon dead layer in the front of the active volume, d_B, the dead-layer thickness behind the active volume, and r, the radius of the active volume, which we required to be less than the manufacturer-specified radius of the complete silicon crystal. Likewise, we set the length of the active volume equal to the manufacturer-specified length of the silicon crystal diminished by the sum of d_F and d_B. We also elected to adjust the distance D between the front active surface of the silicon crystal and the front of the detector cap, which was not precisely specified.

TABLE II. Accepted specifications for our Si(Li) detector.

Quantity	Value
Fixed:	
Be window thickness	0.0254 mm
Be window radius	6.95 mm
Au layer thickness	200 Å
Si crystal length	5.5 mm
Si crystal radius	3 mm
Al collimator inner radius	3 mm
Al collimator length	2.5 mm
Al detector cap outer radius	3.63 cm
Al detector cap thickness	0.13 mm
Optimized:	
d_F, Si front dead layer thickness	0.069 mm
d_B, Si back dead layer thickness	0.534 mm
r, active Si radius	2.634 mm
D, distance, active Si to detector front	8.602 mm

The remaining geometric parameters of the detector were deemed reasonable and/or not critical in the calculation of $\epsilon_\gamma/\epsilon_K$ and therefore were accepted without modifications. These parameters are listed as "fixed" in Table II. Our model also included a thick aluminum collar snugly surrounding the outer circumference of the silicon crystal, and extending into a 2.5-mm long collimator on its front side, as well as a thick aluminum mounting plate located immediately behind the crystal. In our model, for the sake of simplicity, these aluminum pieces extended radially all the way to the inner surface of the detector cap.

The optimized values of d_F, D, d_B, and r were determined to be those for which CYLTRAN calculations matched the measured values of $\epsilon_{23}/\epsilon'_{23}$, ϵ_{23}, ϵ_{88}, and $\epsilon_{12}/\epsilon_{60}$, which had been obtained as described in Sec. IV C 1. The search process was facilitated by the fact that the first three parameters each had the primary impact on a different calculated quantity: d_F predominantly affected the calculated value of ϵ_{23}; D affected $\epsilon_{23}/\epsilon'_{23}$; and d_B affected ϵ_{88}. Our iterative fitting procedure began with a selected value of r. Next, using this value for r, we fixed D at the value that produced an exact match between the CYLTRAN calculations and the measured value of the $\epsilon_{23}/\epsilon'_{23}$ ratio.[3] Then, the values of d_F and d_B were adjusted to reproduce the measured values of ϵ_{23} and ϵ_{88}. Finally, using

[3]For proper comparison, the measured values of both ϵ_{23} and ϵ'_{23} were adjusted for the observed losses due to random summing, because these losses, although small, depend on the acquisition rate (thus affecting ϵ'_{23} more than ϵ_{23}). Furthermore, they depend on the way the detector signals are processed and are not otherwise taken into account in the calculations.

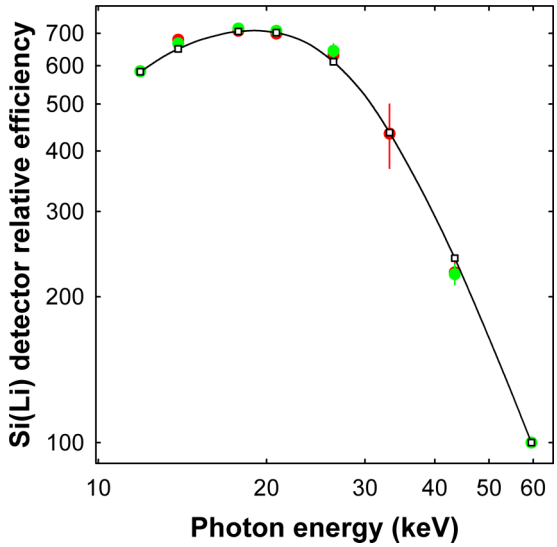

FIG. 8. Measured and CYLTRAN-calculated efficiencies for our Si(Li) detector. The green (red) solid circles represent relative efficiencies measured using our primary (secondary) ^{241}Am source. Note that the green circles and the red circles (almost) completely overlap. The smaller black hollow squares show scaled results of the calculations with the CYLTRAN Monte Carlo code for the source diameter of 3 mm and the source-to-detector distance of 15.9 mm. The black line, which connects the calculated values, is simply to guide the eye. All results have been normalized to 100 for the efficiency at 59.54 keV.

that set of values for r, D, d_F, and d_B we calculated $\epsilon_{12}/\epsilon_{60}$. If the result was greater than (less than) the experimental value, we repeated the procedure using a larger (smaller) value for r. Eventually, we obtained the values of r, D, d_F, and d_B that led to best agreement with experiment; they appear as the "optimized" values listed in Table II.

Our value of D is about 1.6 mm greater than the manufacturer's nominal value of 7 mm, but is not implausible considering the method used by the manufacturer to assemble the detector (see Ref. [30]). The values of d_F and d_B, and the difference between the silicon crystal radius and r (0.366 mm) are all somewhat larger than we expected, but they are not unusual (see, for example, Refs. [43,44]).

In addition to the calibration peaks at 11.89 and 59.54 keV, the measured ^{241}Am spectra contained additional peaks and peak structures at energies of 13.90 keV (Np L_α), 17.81 keV (Np $L_{\beta,\eta}$), 20.82 keV (Np L_γ), 26.34 keV (γ_{26}), 33.20 keV (γ_{33}), and 43.42 keV (γ_{43}). They were used to validate the detector's relative efficiencies as calculated with the parameters tabulated in Table II. The emission probabilities per ^{241}Am decay were taken from the latest available evaluation [45] and all measured efficiencies included correction for self-absorption. The results for both ^{241}Am sources are shown in Fig. 8 where the agreement between calculated and measured relative efficiencies can be seen to be excellent.

4. Effect of the source size on the detector's efficiency

It should be pointed out that the most critical geometric parameters of our Si(Li) detector were determined from measurements with well-centered sources of ^{109}Cd and ^{241}Am, which were shaped like thin discs with 3-mm diameters. Hence the source diameters were considerably smaller than the diameter of the active silicon crystal and the source-to-crystal distances used. Consequently, our source measurements were rather insensitive to the geometric parameters of the detector's supporting structure.

This might not be the case for our ^{93m}Nb source, the diameter of which was much larger: 17 mm. Of course the CYLTRAN Monte Carlo code took account of the larger source diameter but we needed to assure ourselves that the geometrical model properly accounted for the detection efficiency for source components that were as much as 8.5 mm off axis. To test this we measured a succession of spectra with our almost point-like sources placed horizontally off-axis by as much as 24 mm on either side of the central axis.

Measurements of silver K x rays from the ^{109}Cd source were made at a source-to-detector distance of 5.0 mm and horizontal displacements ranging from −24 to 24 mm in steps of 3 mm. The same displacement steps within the same range were also made with the primary ^{241}Am source but in its case the source-to-detector distance was 15.9 mm and we analyzed all major peaks in the spectrum. Both sets of results were compared to CYLTRAN calculations and found to be in satisfactory agreement, which confirms that our geometrical model is valid for Monte Carlo analysis of the 17-mm diameter ^{93m}Nb source.

5. Determination of $\epsilon_\gamma/\epsilon_K$

We are now in a position to use CYLTRAN to calculate the efficiencies for niobium K x rays and 30.8 keV γ rays, using the actual position and size of the ^{93m}Nb source. Since the precision of our measurement is limited to a few percent by counting statistics for the ^{93m}Nb γ-ray peak, we do not require extreme precision in the Si(Li)-detector efficiency. Furthermore it is not the absolute efficiencies but only the relative efficiency ($\epsilon_\gamma/\epsilon_K$) that is used in Eq. (1).

We assessed the uncertainty of the relative efficiency by varying d_F, D, d_B, and r, individually and simultaneously, and monitoring the effect these variations had on the relative efficiency $\epsilon_\gamma/\epsilon_K$ calculated by CYLTRAN. The variations of d_F, D, d_B, and r were limited by the uncertainties of the absolute and relative efficiencies for the K x rays of silver and for the 88-keV γ rays of ^{109m}Ag measured at the source-to-detector distance of 10.2 mm (i.e., ϵ_{23}, ϵ_{88}, and $\epsilon_{88}/\epsilon_{23}$), and also by the uncertainty of $\epsilon_{12}/\epsilon_{60}$. With this procedure our CYLTRAN calculations yielded $\epsilon_\gamma/\epsilon_K = 0.7282(70)$. However, these calculations did not account for the absorption within the niobium source. We account for this effect by using the result obtained in Sec. III A. Upon its inclusion, the value of $\epsilon_\gamma/\epsilon_K$ becomes 0.7263(70) and this is the value to be used in Eq. (1). Its relative uncertainty is just under 1%, more than adequate for our purposes.

V. RESULTS AND DISCUSSION

Table III lists quantities required to determine α_K from Eq. (1). However, given the ambiguity in ω_K, which we noted

TABLE III. Values of the quantities needed to determine α_K from Eq. (1).

Quantity	Value	Percentage uncertainty	Source
N_γ	$1.584(56) \times 10^4$	3.5	Sec. IV B
N_K	$4.1935(23) \times 10^8$	0.055	Sec. IV B
$\epsilon_\gamma/\epsilon_K$	0.7263(70)	0.97	Sec. IV C 5
$\alpha_K \cdot \omega_K$	1.92(7)	3.7	
ω_K[preferred]	0.751(4)	0.53	[27], Sec. II
α_K[preferred]	$2.56(9) \times 10^4$	3.7	
ω_K[alternative]	0.728(9)	1.4	[26], Sec. II
α_K[alternative]	$2.64(10) \times 10^4$	3.9	

in Sec. II, it is important to point out that the result of our measurement is strictly limited to the value of

$$\alpha_K \omega_K = 1.92(7) \times 10^4. \quad (3)$$

To proceed further to extract a result for α_K, we must select a value for ω_K and, as explained in Sec. II, our preference is for the one recommended by Schönfeld and Janssen [27], which was based on their systematic study of 90 elements. In that case we obtain

$$\alpha_K = 2.56(9) \times 10^4, \quad (4)$$

a result with relative uncertainty of ±3.7%. This uncertainty is dominated by the contribution from counting statistics of the weak 30.8-keV γ ray, even after 156 d of data accumulation. Our result for α_K agrees with, but is more precise than one of the previous measurements, which obtained $2.58(15) \times 10^4$ [17], and disagrees strongly with the other, less precise result of $1.7(3) \times 10^4$ [18].

For comparison, Table III also shows the value that α_K would take if the alternative ω_K value, which was based on experimental measurements of niobium alone, were to be used instead. Even though this choice of ω_K has a significantly larger uncertainty than our preferred choice, it only barely increases the counting-statistics-dominated uncertainty on α_K. The shift in the central value for α_K is just under one standard deviation.

Our experimental α_K value from Eq. (4) is compared with three different theoretical calculations in Table IV. All three calculations have been made within the Dirac-Fock framework, but one ignores the presence of the K-shell vacancy while the other two include it in different approximations: the frozen-orbital (FO) approximation, in which it is assumed that the atomic orbitals do not relax after the K electron's removal; and the self-consistent field (SCF) approximation, in which the final-state continuum wave function is calculated in the SCF of the ion, under the assumption that the ion orbitals have fully relaxed. The uncertainties quoted on the theoretical values reflect the uncertainty in the transition energy, 30 760(5) eV (see Table I).

Our result is in excellent agreement with both vacancy approximations and in disagreement by 1.7 standard deviations with the calculation in which vacancy effects are ignored. Were we to use the alternative value for ω_K, we see from Table III that α_K would increase to 2.64(10), so the Δ percentages in Table IV would each increase by a little over 3 units. The agreement with the vacancy approximations would remain, although the frozen-orbital choice would now be favored, and the disagreement with the no-vacancy calculation would increase to 2.4 standard deviations. Thus there is no ambiguity that our experimental result validates only the ICC calculations in which the K-shell vacancy is accounted for in the final state.

TABLE IV. Comparison of the measured α_K value, Eq. (4), for the 30 760(5)-eV $M4$ isomeric transition in ^{93}Nb with calculated values based on different theoretical models for dealing with the K-shell vacancy. Shown also are the percentage deviations, Δ, from the experimental value calculated as (experiment-theory)/theory. For a description of the various models used to determine the conversion coefficients, see the text and Ref. [5].

Model	α_K	Δ(%)
Experiment	$2.56(9) \times 10^4$	
Theory:		
No vacancy	$2.396(1) \times 10^4$	+6.8(40)
Vacancy, frozen orbitals	$2.599(1) \times 10^4$	– 1.5(36)
Vacancy, SCF of ion	$2.544(1) \times 10^4$	+0.6(37)

This result is not unexpected. For the ^{93m}Nb isomer, the kinetic energy of the converted K electron is about 12 keV, and so it takes the electron about 2 attoseconds to travel the distance equal to the radius of the atom (which is on the order of 1 Å). In contrast, the width of the niobium K level is about 4 eV [3], from which we can deduce that the average lifetime of a K vacancy is about 100 attoseconds, i.e., about 50 times longer than the time it takes the conversion electron to leave the atom. Therefore, the effects associated with the presence of the K vacancy in the final state are significant and, as confirmed by our experiment, cannot be ignored.

We note that an $M4$ transition between $(1/2)^-$ and $(9/2)^+$ states can in principle also include a small contribution of $E5$ multipolarity. In the case of the 30.76-keV transition in ^{93}Nb, the α_K value for $E5$ is only about 10% smaller than it is for $M4$, and its dependence on the presence of the K-shell vacancy is about the same [46]. Therefore a small admixture of $E5$ multipolarity, if it existed, would have a negligible effect on our calculated values of α_K and have no impact on our conclusions.

VI. CONCLUSIONS

We have measured the K-shell internal conversion coefficient, α_K, for the $M4$ decay of the 30.8 keV isomer in ^{93}Nb with a relative uncertainty of ±3.7%. Our result, $2.56(9) \times 10^4$, agrees with internal-conversion calculations that take into account effects due to the presence of the K vacancy in the final state, and disagrees by 1.7 standard deviations with the calculation in which these effects are ignored.

The need to include K-vacancy effects in the calculations has also been indicated by nine previous measurements of internal conversion coefficients undertaken by the present group of authors [4–13], and from the only three other precise

measurements performed elsewhere [2,15,16], all involving $E3$ or $M4$ transitions. These have already spanned a wide range of elements, $45 \leqslant Z \leqslant 80$. The $M4$ transition in ^{93}Nb ($Z = 41$), reported on here, represents the lowest atomic number, the lowest transition energy, and the highest α_K value measured and tested so far.

Our study has additionally drawn attention to an existing ambiguity in the literature values for the fluorescence yield, ω_K, for niobium. In the face of this ambiguity, we have chosen to follow the same practice as in our previous work on high-multipolarity transitions, in which we used the ω_K values tabulated by Schönfeld and Janssen [27], who based their values on a systematic study of experimental results from 90 elements. Importantly, although the value of α_K is influenced by this choice, our conclusions about the ICC calculations are not. If, in the future, the value for niobium's fluorescence yield is definitively established, a new value for α_K can readily be obtained from Eq. (3), which encapsulates our basic experimental result.

In the course of this work we also determined the $M4$ transition energy in ^{93m}Nb to be 30 760(5) eV. The relative uncertainty of our result is smaller by about a factor of four than that of the currently accepted value [19].

ACKNOWLEDGMENTS

The authors thank Dr. Y. Bisrat for sample characterizations by means of SEM and EDS, and Dr. J. Wu for the measurements using XPS, all performed at the Texas A&M University Materials Characterization Facility. This report is based upon work supported by the U.S. Department of Energy, Office of Science, Office of Nuclear Physics, under Award No. DE-FG03-93ER40773, and by the Robert A. Welch Foundation under Grant No. A-1397.

[1] I. M. Band, M. B. Trzhaskovskaya, C. W. Nestor, Jr., P. Tikkanen, and S. Raman, At. Data Nucl. Data Tables **81**, 1 (2002).
[2] S. Raman, C. W. Nestor, Jr., A. Ichihara, and M. B. Trzhaskovskaya, Phys. Rev. C **66**, 044312 (2002), see also the electronic addendum to this paper, the location of which is given in the paper's Ref. [32].
[3] J. L. Campbell and T. Papp, At. Data Nucl. Data Tables **77**, 1 (2001).
[4] N. Nica, J. C. Hardy, V. E. Iacob, M. Bencomo, V. Horvat, H. I. Park, M. Maguire, S. Miller, and M. B. Trzhaskovskaya, Phys. Rev. C **89**, 014303 (2014).
[5] N. Nica, J. C. Hardy, V. E. Iacob, S. Raman, C. W. Nestor, Jr., and M. B. Trzhaskovskaya, Phys. Rev. C **70**, 054305 (2004).
[6] N. Nica, J. C. Hardy, V. E. Iacob, J. R. Montague, and M. B. Trzhaskovskaya, Phys. Rev. C **71**, 054320 (2005).
[7] N. Nica, J. C. Hardy, V. E. Iacob, W. E. Rockwell, and M. B. Trzhaskovskaya, Phys. Rev. C **75**, 024308 (2007).
[8] N. Nica, J. C. Hardy, V. E. Iacob, C. Balonek, and M. B. Trzhaskovskaya, Phys. Rev. C **77**, 034306 (2008).
[9] N. Nica, J. C. Hardy, V. E. Iacob, J. Goodwin, C. Balonek, M. Hernberg, J. Nolan, and M. B. Trzhaskovskaya, Phys. Rev. C **80**, 064314 (2009).
[10] N. Nica, J. C. Hardy, V. E. Iacob, T. A. Werke, C. M. Folden III, L. Pineda, and M. B. Trzhaskovskaya, Phys. Rev. C **93**, 034305 (2016).
[11] N. Nica, J. C. Hardy, V. E. Iacob, T. A. Werke, C. M. Folden III, K. Ofodile, and M. B. Trzhaskovskaya, Phys. Rev. C **95**, 064301 (2017).
[12] N. Nica, J. C. Hardy, V. E. Iacob, H. I. Park, K. Brandenburg, and M. B. Trzhaskovskaya, Phys. Rev. C **95**, 034325 (2017).
[13] N. Nica, J. C. Hardy, V. E. Iacob, V. Horvat, H. I. Park, T. A. Werke, K. J. Glennon, C. M. Folden III, V. I. Sabla, J. B. Bryant, X. K. James, and M. B. Trzhaskovskaya, Phys. Rev. C **98**, 054321 (2018).
[14] J. C. Hardy, N. Nica, V. E. Iacob, and M. B. Trzhaskovskaya, Appl. Radiat. Isot. **134**, 406 (2018).
[15] H. H. Hansen, E. de Roost, W. Van der Eijk, and R. Vaninbroukx, Z. Phys. **269**, 155 (1974).
[16] I. N. Vishnevsky, V. A. Zheltonozhsky, and M. A. Ukhin, Izv. Akad. Nauk SSSR, Ser. Fiz. **51**, 863 (1987) [Bull. Acad. Sci. USSR, Phys. Ser. **51**, 23 (1987)].
[17] M. Jurčević, A. Ljubičić, and D. Rendić, Fizika **8**, 81 (1976).
[18] J. Morel, J.-P. Perolat, and N. Coursol, C. R. Acad. Sci. (Paris) B **284**, 223 (1977).
[19] C. M. Baglin, Nucl. Data Sheets **112**, 1163 (2011).
[20] P. R. Gray, Phys. Rev. **101**, 1306 (1956).
[21] C. E. Roos, Phys. Rev. **105**, 931 (1957).
[22] S. K. Arora, K. L. Allawadhi, and B. S. Sood, Physica B + C (Amsterdam) **111**, 71 (1981).
[23] S. Singh, R. Rani, D. Mehta, N. Singh, P. C. Mangal, and P. N. Trehan, X-Ray Spectrometry **19**, 155 (1990).
[24] R. Durak and Y. Özdemir, Radiat. Phys. Chem. **61**, 19 (2001).
[25] I. Han, M. Sahin, L. Demir, and Y. Sahin, Appl. Radiat. Isot. **65**, 669 (2007).
[26] J. Riffaud, M.-C. Lépy, Y. Ménesguen, and A. Novikova, X-Ray Spectrometry **46**, 341 (2017).
[27] E. Schönfeld and H. Janssen, Nucl. Instrum. Methods Phys. Res. A **369**, 527 (1996).
[28] D. A. Mayorov, E. E. Tereshatov, T. A. Werke, M. M. Frey, and C. M. Folden III, Nucl. Instrum. Methods Phys. Res. B **407**, 256 (2017).
[29] C. T. Chantler, K. Olsen, R. A. Dragoset, J. Chang, A. R. Kishore, S. A. Kotochigova, and D. S. Zucker, X-Ray Form Factor, Attenuation and Scattering Tables (version 2.1) (2005), available online at http://physics.nist.gov/ffast.
[30] R. G. Helmer, N. Nica, J. C. Hardy, and V. E. Iacob, Appl. Radiat. Isot. **60**, 173 (2004), and references therein.
[31] EG&G ORTEC, model SLP-06165-P, Ser. No. 34-T7263.
[32] https://www.ortec-online.com/products/electronics/multichannel-analyzers-mca/basic-analog/easy-mca-2k-or-8k.
[33] https://www.ortec-online.com/products/application-software/maestro-mca.
[34] R. D. Deslattes, E. G. Kessler, Jr., P. Indelicato, L. de Billy, E. Lindroth, and J. Anton, Rev. Mod. Phys. **75**, 35 (2003).
[35] R. G. Helmer and C. van der Leun, Nucl. Instrum. Methods Phys. Res. A **450**, 35 (2000).
[36] E. Schönfeld and G. Rodloff, PTB Report No. PTB-6.11-1999-1 (1999).

[37] C. Herren and J.-C. Dousse, Phys. Rev. A **53**, 717 (1996).
[38] C. Herren and J.-C. Dousse, Phys. Rev. A **56**, 2750 (1997).
[39] K. Debertin and R. Helmer, *Gamma- and X-ray Spectrometry with Semiconductor Detectors* (Elsevier, Amsterdam, 2001).
[40] J. A. Halbleib and T. A. Mehlhorn, Nucl. Sci. Eng. **92**, 338 (1986); J. A. Halbleib, R. P. Kensek, T. A. Mehlhorn, G. D. Valdez, S. M. Seltzer, and M. J. Berger, CYLTRAN 3.0, Sandia National Labs (Albuquerque, NM), Report No. SAND91-1634 (1992).
[41] M. J. Berger, J. H. Hubbell, S. M. Seltzer, J. Chang, J. S. Coursey, R. Sukumar, D. S. Zucker, and K. Olsen, XCOM: Online Photon Cross Section Database (version 1.5), available online at http://physics.nist.gov/xcom.
[42] J. S. Hansen, J. C. McGeorge, D. Nix, W. D. Schmidt-Ott, I. Unus, and R. W. Fink, Nucl. Instrum. Methods **106**, 365 (1973).
[43] M. Mesradi, E. Elanique, A. Nourreddine, A. Pape, D. Raiser, and A. Sellam, Appl. Radiat. Isot. **66**, 780 (2008).
[44] H. D. Choung, N. T. T. Linh, L. T. N. Trang, V. H. Nguyen, L. H. Minh, C. T. Tai, and T. T. Thanh, Rad. Phys. Chem. **166**, 108459 (2020).
[45] V. P. Chechev and N. K. Kuzmenko, Appl. Radiat. Isot. **68**, 1578 (2010).
[46] http://bricc.anu.edu.au/index.php.